Scientific Research Publishing

Engineering, 2025, 17(4), 259-275
https://www.scirp.org/journal/eng
ISSN Online: 1947-394X
ISSN Print: 1947-3931

Modelling of Indirect Solar Drying with and without a Thermal Storage Unit for Tomatoes

Salifou Tera[1*], Souleymane Sinon[2], Mamadi Diakite[1], Kalil Pierre Mathos[1], Oumar Sanogo[2]

[1]Département de Physique, Faculté des Sciences et Techniques, Université de N'Zérékoré, N'Zérékoré, République de Guinée
[2]Institut de Recherche en Sciences Appliquées et Technologies, Centre National de la Recherche Scientifique et Technologique (IRSAT/CNRST), Ouagadougou, Burkina Faso
Email: *salifoutera@gmail.com

How to cite this paper: Tera, S., Sinon, S., Diakite, M., Mathos, K.P. and Sanogo, O. (2025) Modelling of Indirect Solar Drying with and without a Thermal Storage Unit for Tomatoes. *Engineering*, **17**, 259-275.
https://doi.org/10.4236/eng.2025.174016

Received: November 19, 2024
Accepted: April 6, 2025
Published: April 9, 2025

Abstract

The present work presents indirect solar drying with or without a tomato drying unit and the mathematical modelling of the indirect solar drying system with or without a storage unit. Heat and mass transfer equations were used to predict the thermal behaviour of solar drying with or without a tomato unit. During the experiment, the tomatoes were dried to an average final moisture content of 0.12 kg_{water}/kg_{ms} with an average initial water content of 17.6 kg_{water}/kg_{ms}. The experimental data were fitted to eight (08) different mathematical thin film drying models. These models were compared using the coefficient of determination R^2, Ki-square χ^2 and the square root of the root mean square error RMSE. The results show that Page's model best describes the drying curve characteristic of tomatoes. This Page's model gives a higher value of determination $R^2 = 0.9942$ and lower values of Ki-square $\chi^2 = 0.02797$ and RMSE = 0.00704, compared with the seven (07) other mathematical methods used to describe the thermal behavior of tomato solar drying.

Keywords

Tomato, Solar Drying, Thermal Storage, Mathematical Model, Moisture Content

1. Introduction

Solar drying of agri-food products is an important preservation method that can be applied to many agricultural products. This type of drying results in considerable savings, as the energy source is free and renewable [1]. However, this drying technique is extremely dependent on sunshine and weather conditions. What's

more, the drying time required for a given load can be quite long for a number of products with a high water content, such as tomatoes, mangoes, etc.... The integration of a storage system into indirect solar dryers makes it possible to compensate for the unavailability of solar energy and to ensure that the drying process continues beyond the hours of sunshine [2].

Large-scale testing of different products and system configurations is sometimes costly and sometimes impossible. Sizing, drying system efficiency or design optimization can be assessed or achieved through parametric study. The development of a simulation model is a valuable tool for predicting the performance of solar drying systems [3]. Several researchers have carried out simulation studies on various solar drying systems [1] [4]-[9].

A.A. El-Sebaii *et al*. [3] presented an experimental and theoretical study on empirical correlations in the drying kinetics of certain fruits and vegetables. An indirect solar dryer operating by natural convection was developed. The experimental data were used to calculate the drying constants of the selected products. The proposed mathematical model is based on the energy and mass conservation equations and uses the proposed correlations and constant values. Kamil Sacilik *et al*. [5] carried out a mathematical modelling study on a solar tunnel dryer for thin-film drying of organic tomatoes. A non-linear regression method was used to fit 10 different mathematical models proposed in the literature to experimental thin film drying curves. They found that the Diffusion Approximation model showed a better fit for the experimental drying data than the other models. Ibrahim Doymaz [10] reported a study on the characteristics of tomato drying air. He found that increasing the temperature of the drying air from 55˚C to 70˚C resulted in a significant increase in the drying rate of the tomato. The experimental data were then fitted to the Henderson and Pabis model and Page model. The results showed that Page's model gave a better description of tomato drying kinetics. Inci Turk Togrul *et al*. [1] presented a study on the modelling of apricot drying kinetics. Variations in drying rate as a function of time and water content in apricots were used to test fourteen different thin-film drying models presented in the literature, and a new model was developed. Among the models used according to the authors, the logarithmic model proved to be the best for explaining the drying behaviour of apricots.

The aim of this study is to propose an experimental and modeling study on empirical correlations of tomato drying kinetics. Two types of solar dryers are studied: an indirect solar dryer and an indirect solar dryer with thermal energy storage. The theoretical results of the characterization of tomato drying kinetics were compared with the experimental results.

2. Description and Operating Principle of the Device

The solar dryer system consists mainly of two flat-plate solar air collectors ((1) and (2)) which convert the sun's rays into thermal energy, a drying chamber (3) containing the products to be dried, and a cylindrical thermal storage unit (4)

(Figure 1). Crushed and calibrated granite is used as the storage material. Figure 1 shows the loading phase of the storage tank and the drying phase of the product (tomatoes). During the day, air heated by the solar collector (1) is sent to the drying chamber. As it circulates inside the drying chamber, it transfers its heat to the product and recovers the moisture released by the product. It exits the drying chamber through the chimney, having cooled down. At the same time, the air heated by the solar collector (2) is sent by forced convection to the storage tank by means of a fan placed at the solar collector inlet. The airflow enters the tank from above, transferring its heat to the granite balls inside the tank. It exits cooled by the base of the tank. During the discharge and drying phase (at night), cold air enters from the bottom of the storage by forced convection. It heats up on contact with the granite balls before entering the drying chamber to continue the drying process (Figure 2). The characteristics of the solar collectors, the storage tank, the chamber and the physical properties of the heat transfer fluid (air) are given in Tables 1-4 respectively.

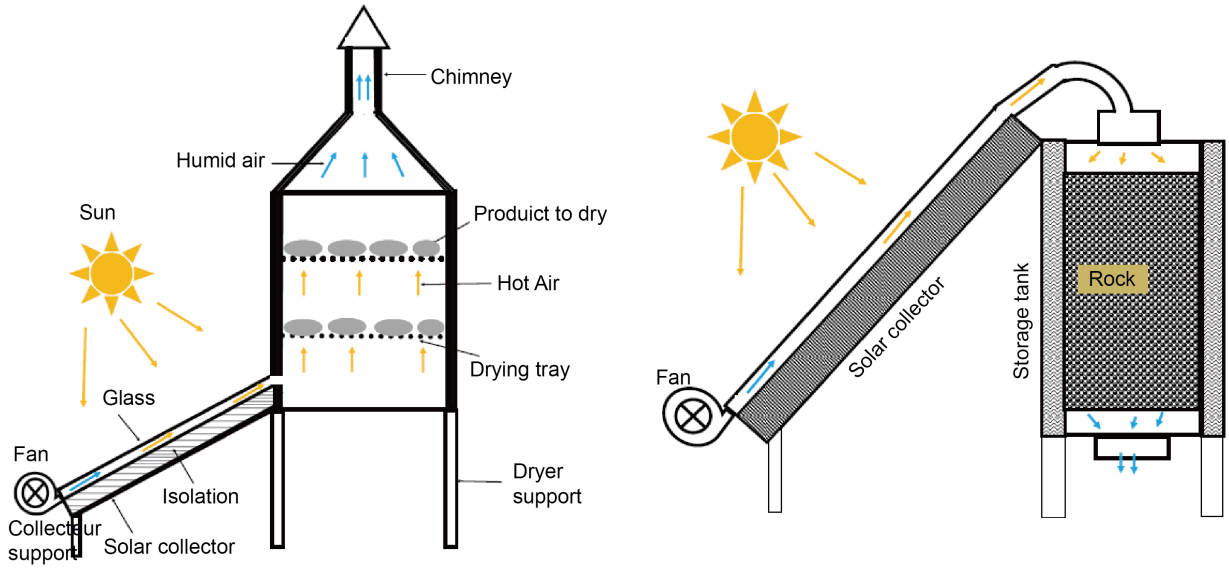

Figure 1. Charging and drying phase during the day.

Table 1. Characteristics of solar air collectors.

Parameter	Value
Collector 1 area (m^2)	3.69
Collector 2 area (m^2)	1.56
Absorber coating	Black mat paint
Glass envelope	Low-iron glass
Masse flow rate (kg/s)	0.018
Collector slope angle	12˚

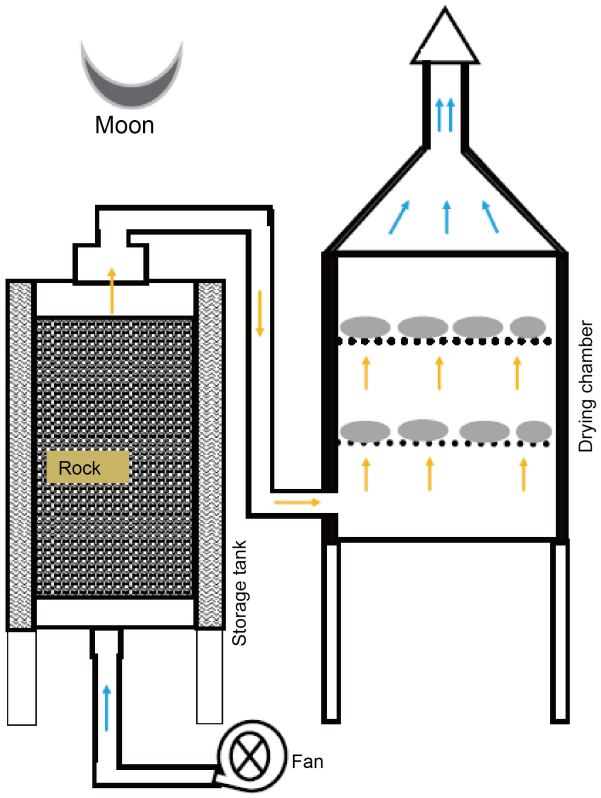

Figure 2. Discharge and drying phase overnight.

Table 2. Characteristics of the rock bed.

Parameter	Value
Length of rock bed (m)	1.8
Cross sectional area of the rock bed (m)	0.5
Volume of the rock bed (m^3)	0.15
Specific heat of the rock (J/kg·K)	950
Apparent rock bed density (kg/m^3)	2775
Effective thermal conductivity (w/m·K)	2.61
Bed void fraction	0.53
Sphericity of rock bed	0.7
Masse flow rate (kg/s)	0.010

Table 3. Characteristics of a drying chamber.

Parameter	Value
Length (m)	0.5
Width (m)	0.5
Height (m)	1
Volume of the drying chamber (m^3)	0.25

Table 4. Physical properties of air [1].

Parameter	Value
Specific heat of the air (J/kg·K)	$-2.3397 \times 10^{-7} \times T(K)^3 + 5.5136.10^4 \times T(K)^2 - 0.19523 \times T(K) + 1019.9050$
Air density (kg/m³)	$101325 \times M/(8.3145 \times T(K))$ $M = 0.028971$ kg·mol^{-1}
Thermal conductivity (w/m·K)	$1.521 \times 10^{-11} \times T(K)^3 - 4.857 \times 10^{-8} \times T(K)^{-2} + 1.0184 \times 10^{-4} \times T(K) - 3.9333 \times 10^{-4}$

3. Experiment Procedure

The tomatoes used in our experiment were bought fresh from the local market and selected uniformly on the basis of very specific criteria [2]. These criteria included size, degree of ripeness and external shape. The selected tomatoes were washed in lukewarm water to remove impurities, then cut into 1 cm-thick slices. The sliced tomatoes were placed on the various trays (around 1.125 kg for each tray). The experimental measurement protocol consisted mainly of measuring temperature, relative humidity, sample mass and drying air velocity. The initial water content was calculated by taking three different samples. The air speed at the entrance to the drying chamber was set at 1 m/s. The drying experiments during sunny periods lasted about 10 hours, and those carried out with the storage tank lasted about 6 hours. The experiments were repeated three times and an average value was taken for the analyses. The process is stopped when the wet mass of the product reaches its final moisture content of around 11%. To determine the dry mass of the product, samples were taken from the racks at the end of the drying process. These samples were weighed and placed in an oven at 70˚C for 24 hours.

4. Process Modelling

4.1. Thermocline Storage Modelling

A three-equation, one-dimensional thermal model developed by Esence [11] and Fasquelle [12] is used in this study to predict the thermal behavior of our sensitive storage system. It implements 3 balance equations performed at the level of the fluid (1), the solid storage material (2), and the tank walls (3). The pebbles are considered to behave like thin bodies (uniform temperature).

$$\varepsilon\left(\frac{\partial\left(\rho_f C_{P_f} T_f\right)}{\partial t} + \frac{\partial\left(\rho_f u_f C_{P_f} T_f\right)}{\partial z}\right) = \frac{\partial}{\partial z}\left(\lambda_{eff,f}\frac{\partial T_f}{\partial z}\right) + h_{eff,f\text{-}s} a_s \left(T_s - T_f\right) + h_{eff,f\text{-}p} a_{P,int}\left(T_P - T_f\right) \quad (1)$$

$$(1-\varepsilon)\rho_s C_{P_s}\frac{\partial T_s}{\partial t} = \frac{\partial}{\partial z}\left(\lambda_{eff,s}\frac{\partial T_s}{\partial z}\right) + h_{eff,f\text{-}s} a_s\left(T_f - T_s\right) \quad (2)$$

$$\rho_P C_{P_P}\frac{\partial}{\partial t} = \frac{\partial}{\partial z}\left(\lambda_P\frac{\partial T_P}{\partial z}\right) + h_{eff,f\text{-}p} a_{p,int}\left(T_f - T_P\right) + U_P a_{p,ex}\left(T_{ex} - T_P\right) \quad (3)$$

The rock bed is treated as a continuous medium. The effective thermal conductivities of the fluid and solid are given by Equations (4) and (5).

$$\lambda_{eff,f} = \varepsilon \lambda_f \tag{4}$$

$$\lambda_{eff,s} = (1-\varepsilon)\lambda_s \tag{5}$$

The Reynolds number characteristic of the flows (6) is based on the equivalent diameter of the solids making up the bed.

$$Re = \frac{\rho_f u_f \varepsilon d_{eq}}{\mu_f} \tag{6}$$

The Wakao and Faguei correlation recommended by Esence [11] is used to calculate the Nusselt number (7).

$$Nu_s = 2 + 1.1 Re^{0.6} Pr^{1/3} = \frac{h_s d_{eq}}{\lambda_f} \tag{7}$$

The effective rock-fluid exchange coefficient is calculated as a function of the rock-fluid exchange coefficient defined in equation (8) [12].

$$\frac{1}{h_{eff,s}} = \frac{1}{h_s} + \frac{d_{eq}}{10\lambda_s} \tag{8}$$

The effective exchange coefficient between the fluid and the wall can be obtained through the correlations expressed in Equations (9) and (10) [12].

$$Nu_p = \left(1 - 1.5\left(\frac{d_{eq}}{D}\right)^{1.5}\right) Re^{0.59} Pr^{1/3} = \frac{h_p d_{eq}}{\lambda_f} \tag{9}$$

$$\frac{1}{h_{eff,p}} = \frac{1}{h_p} + \frac{e_p}{3\lambda_p} \tag{10}$$

4.2. Modelling of the Solar Collector

To establish the heat balance for each collector component, we applied the nodal method, which consists of dividing each solar collector component into a number of nodes to which temperatures are assigned. In this way, the energy balance was applied to the glass (11), the absorber (12), the heat transfer fluid (13), the insulation (14) and the outer face of the solar collector (15).

$$\begin{aligned} m_v C_{P_v} \frac{\partial T_v}{\partial t} = {} & \alpha_v I_G S_v + h_{cv\text{-}ext} S_v (T_{ex} - T_v) + h_{r,v\text{-}ciel} S_v (T_{ciel} - T_v) \\ & + h_{r,v\text{-}abs} S_{abs} (T_{abs} - T_v) + h_{c,v\text{-}abs} S_v (T_{abs} - T_v) \end{aligned} \tag{11}$$

$$\begin{aligned} m_{abs} C_{P_{abs}} \frac{\partial T_{abs}}{\partial t} = {} & \alpha_{abs} \tau_v I_G S_{abs} + h_{r,abs\text{-}v} S_{abs} (T_v - T_{abs}) + h_{cv,abs\text{-}v} S_{abs} (T_v - T_{abs}) \\ & + h_{cv,abs\text{-}f} S_{abs} (T_f - T_{abs}) + h_{r,abs\text{-}pq} S_{abs} (T_{pq} - T_{abs}) \end{aligned} \tag{12}$$

$$\rho_f C_{P_f} V \left(\frac{\partial T_f}{\partial t} + u_{cap} \frac{\partial T_f}{\partial x}\right) = h_{cv,abs\text{-}f} S_{abs} (T_{abs} - T_f) \tag{13}$$

$$m_{pq} C_{P_{pq}} \frac{\partial T_{pq}}{\partial t} = h_{cd,pq\text{-}iso} S_{pq} (T_{iso} - T_{pq}) + h_{ray,abs\text{-}pq} S_{pq} (T_{abs} - T_{pq}) \tag{14}$$

$$m_{iso}C_{P_{iso}}\frac{\partial T_{iso}}{\partial t}=h_{cd,pq\text{-}iso}S_{iso}\left(T_{pq}-T_{iso}\right)+h_{cv,iso\text{-}ex}S_{iso}\left(T_{ex}-T_{iso}\right) \quad (15)$$

4.3. Modelling of the Drying Chamber

The dryer is divided into a number of fictitious slices in the x direction of flow, defined by the volume delimited by two racks and the walls of the drying chamber (**Figure 3**). The Equations ((16), (17), (18) and (19)) below describe the heat balances at any given slice of the drying chamber.

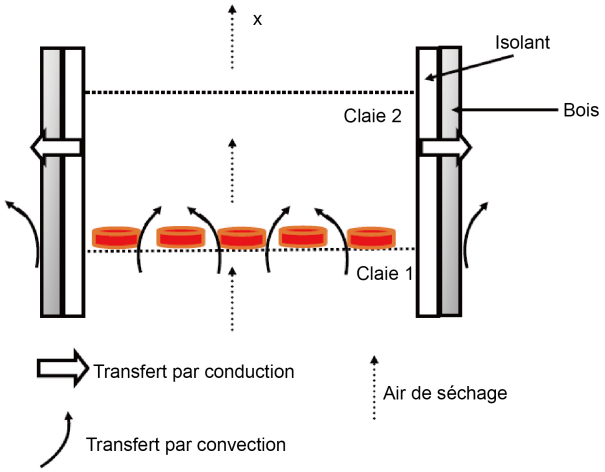

Figure 3. Heat exchange in a dryer section.

$$\dot{m}_{sech}C_{P_f}\Delta x\frac{\partial T_f}{\partial x}=h_{cv,f\text{-}pr}S_{pr}\left(T_{pr}-T_f\right)+h_{cv,f\text{-}pint}S_p\left(T_{P,int}-T_f\right) \quad (16)$$

$$m_{pr}C_{P_{pr}}\frac{\partial T_{pr}}{\partial t}+m_{sech}L_V\frac{\partial X}{\partial t}=h_{cv,pr\text{-}f}S_{pr}\left(T_f-T_{pr}\right) \quad (17)$$

$$m_pC_{P_P}\frac{\partial T_{P,int}}{\partial t}=h_{cd,pint\text{-}pext}S_P\left(T_{Pext}-T_{Pint}\right)+h_{cv,f\text{-}pint}S_P\left(T_f-T_{pint}\right) \quad (18)$$

$$\begin{aligned}m_pC_{P_P}\frac{\partial T_{Pext}}{\partial t}&=h_{cd,pint\text{-}pext}S_P\left(T_{Pint}-T_{Pext}\right)+h_{cv,ex\text{-}pext}S_P\left(T_{ex}-T_{pext}\right)\\&+h_{r,ciel\text{-}pext}S_P\left(T_{ciel}-T_{pext}\right)\end{aligned} \quad (19)$$

The expression $m_{sech}L_V\frac{\partial X}{\partial t}$ defined in Equation (17) above refers to the mass of water evaporated per unit time with m_{sech} the dry mass of the product and $\frac{\partial X}{\partial t}$ product drying speed expressed in kilograms of water per kilogram of dry matter in one second ($kg_{water}/(kg_{ms}/s)$).

4.3.1. Drying Kinetics

The instantaneous water content (X_t) of the tomato samples was transformed into reduced water content (X_r), according to equation (21) defined below [13]-[15]:

$$X_{red} = \frac{X_t - X_{eq}}{X_0 - X_{eq}} \tag{21}$$

where X_0 is the initial water content of the product and X_{eq} is the equilibrium water content of the product. The reduced water content X_{red}, has been simplified using equation (22), since X_{eq} is negligible compared with X_t and X_0 [6].

$$X_{red} = \frac{X_t}{X_0} \tag{22}$$

4.3.2. Modelling of the Drying Kinetics

To simulate tomato drying kinetics, we used empirical models described in the literature. To determine the models, we used the non-linear regression method to establish a correlation giving the evolution of the reduced water content (X_{red}) of tomato samples as a function of time. Fitting was carried out using MATLAB 2022a software. Table 5 presents some empirical models described in the literature.

Table 5. Mathematical models [1] [5].

Model Name	Expression Model
Lewis	$X_{eq} = \exp(-bt)$
Henderson and Pabis	$X_{eq} = a * \exp(-bt)$
Page	$X_{eq} = \exp(-bt^n)$
Logarithmique	$X_{eq} = a * \exp(-bt) + c$
Two terms	$X_{eq} = a * \exp(-bt) + c * \exp(-dt)$
Approach of the diffusion	$X_{eq} = a * \exp(-bt) + (1-a) * \exp(-bct)$
Verma *et al.*	$X_{eq} = a * \exp(-bt) + (1-a) * \exp(-ct)$
Wang and singh	$X_{eq} = 1 + at + bt^2$

4.4. Drying Data Analysis

Page's reduced water content model was fitted to the experimental data, and model parameters were determined using non-linear regression analysis. The criteria for assessing the smoothing quality of the experimental results are the coefficient of determination (R^2), the reduced ki-square (χ^2) and the root mean square error (RMSE) [4] [6]. These parameters are calculated according to the relationships:

$$R^2 = \frac{\sum_{i=1}^{N} \left(X_{red,expi} - X_{red,thi} \right)^2}{\sqrt{\left[\sum_{i=1}^{N} \left(X_{red,expi} - X_{red,thi} \right)^2 \right] * \left[\sum_{i=1}^{N} \left(X_{red,expi} - X_{red,thi} \right)^2 \right]}} \tag{29}$$

$$\chi^2 = \frac{\sum_{i=1}^{N} \left(X_{expi} - X_{thi} \right)^2}{N - n} \tag{30}$$

$$\mathrm{RMSE} = \left[\frac{1}{N} \times \sum_{i=1}^{N} \left(X_{expi} - X_{thi} \right)^2 \right]^{1/2} \tag{31}$$

5. Numerical Resolution

The time terms of the solar collector and drying chamber energy balance equations were discretized using the implicit Euler finite difference method. The equations for the storage tank model were discretized using the one-dimensional finite volume method. Temporal terms in the energy and continuity equation were discretized using the implicit Euler scheme. Diffusive and advective terms are treated by the QUICK scheme [12]. The 2nd-order centered difference scheme was used to discretize the diffusion flow. The numerical resolution of these equations was performed in the SCILAB programming language, using the Newton-Raphson iterative method.

6. Validation of the Thermocline Storage Model

The mathematical models developed were validated using experimental data provided by Cascetta [12]. The experiment involved a process of charging and discharging a storage system with aluminum balls as the storage material and air as the heat transfer fluid. The height and diameter of the tank used by Cascetta are 1.8m and 0.584 m respectively. The porosity of the ball bed is 0.39. A comparison of the numerical results with the experimental data supplied by Cascetta is shown in **Figure 4**. As can be seen from **Figure 4(a)**, the temperature profiles calculated numerically during loading are in perfect agreement with the experimental profiles. **Figure 4(b)** shows the temperature profiles during discharge, with the numerical results in slightly less agreement with the experimental ones (the temperature profiles given by the models are slightly higher at the thermocline than those of the experimental model), while still being very close. This may be due to wall inertia phenomena that were not properly taken into account in the modelling during the discharge phase.

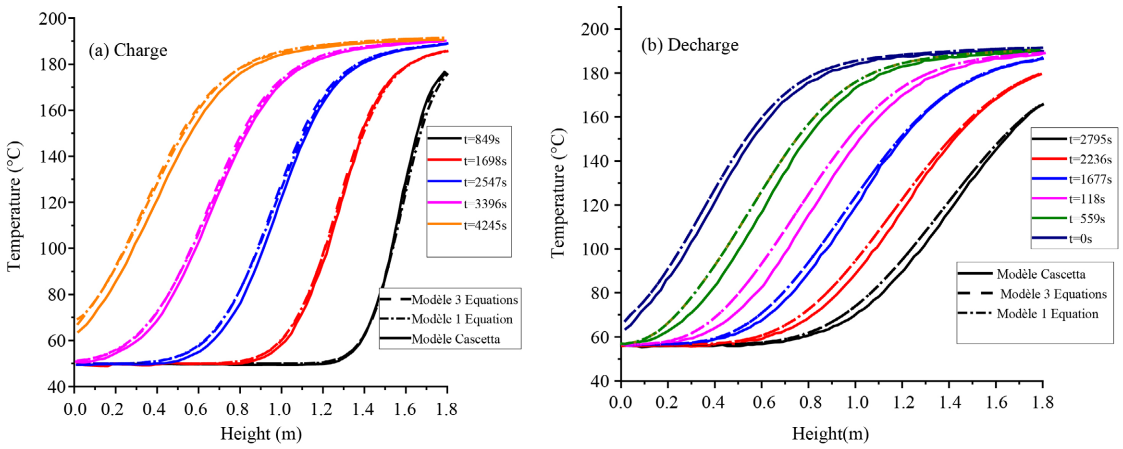

Figure 4. Comparison of the temperature profiles predicted by the model during the charging and discharging phases with Cascetta's experimental results [13].

7. Results and Discussion

7.1. Experimental Results

Figure 5 and Figure 6 show the evolution of experimental tomato water content during indirect solar drying with or without a thermal storage unit on 16-17/03/2023; 19-20/03/2023; 25-26/03/2023 and 31/03/2023-01/04/2023. The evolution of experimental water content in the two drying racks follows a decreasing trend as a function of drying time. The difference between the two trays is relatively small, which means that drying is almost uniform across both trays [2]. During the night, or when the storage tank is put into operation, the water content of the product decreases again until the discharge process stops.

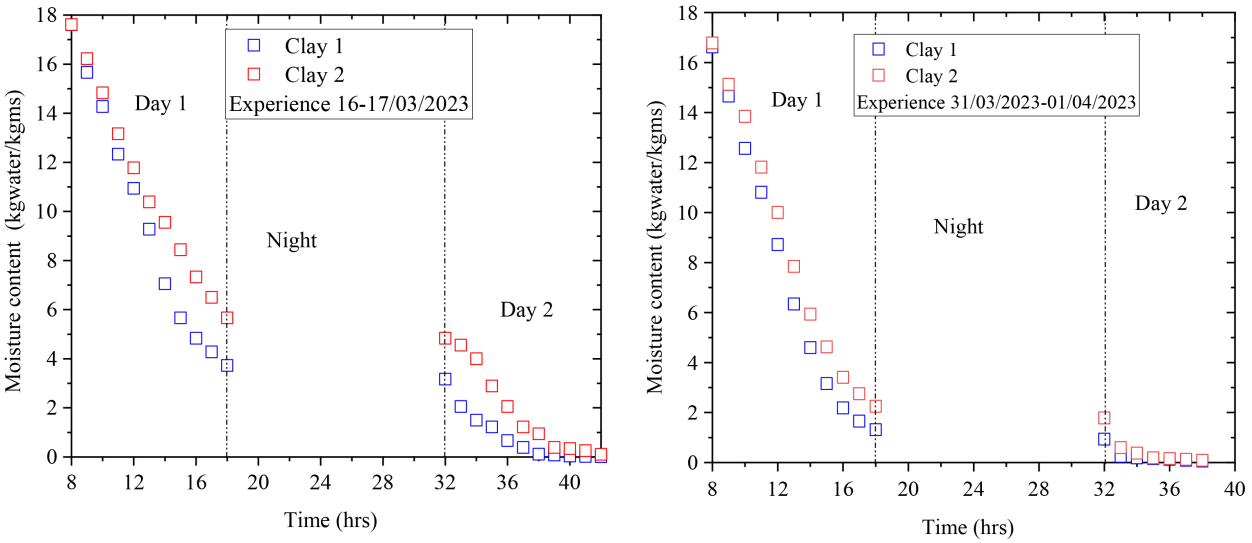

Figure 5. Time-dependent change in product water content during the indirect solar drying process.

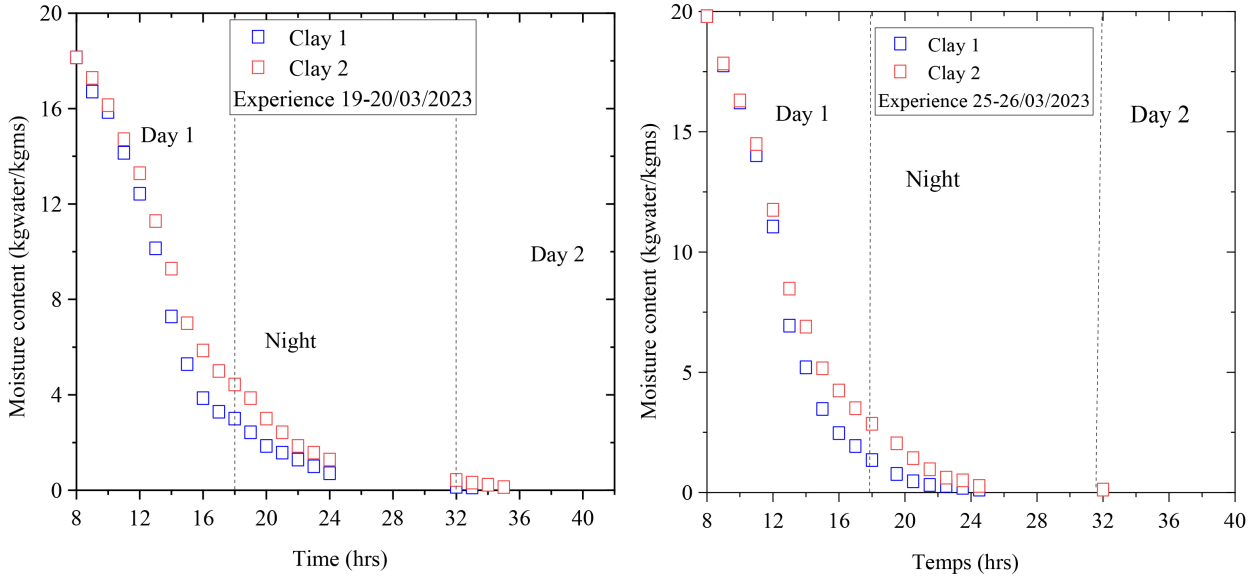

Figure 6. Time-dependent change in product water content during indirect solar drying with thermal storage system.

Figure 7 and Figure 8 show changes in the average water content of tomatoes during solar drying with or without a thermal storage unit on 16-17/03/2023; 19-20/03/2023; 25-26/03/2023 and 31/03/2023 -01/04/2023. The initial dry-base water contents of the product on these different drying days are 17.6 kg_{water}/kg_{ms} (16-17/03/2023); 18.14 kg_{water}/kg_{ms} (19-20/03/2023); 19.8 kg_{water}/kg_{ms} (25-26/03/2023) and 16.8 kg_{water}/kg_{ms} (31/03/2023 -01/04/2023) respectively. And the final moisture content of tomatoes on a dry basis at the end of these different drying days are respectively 0.10 kg_{water}/kg_{ms} (16-17/03/2023); 0.13 kg_{water}/kg_{ms} (19-20/03/2023); 0.115 kg_{water}/kg_{ms} (25-26/03/2023) and 0.15 kg_{water}/kg_{ms} (31/03/2023 -01/04/2023).

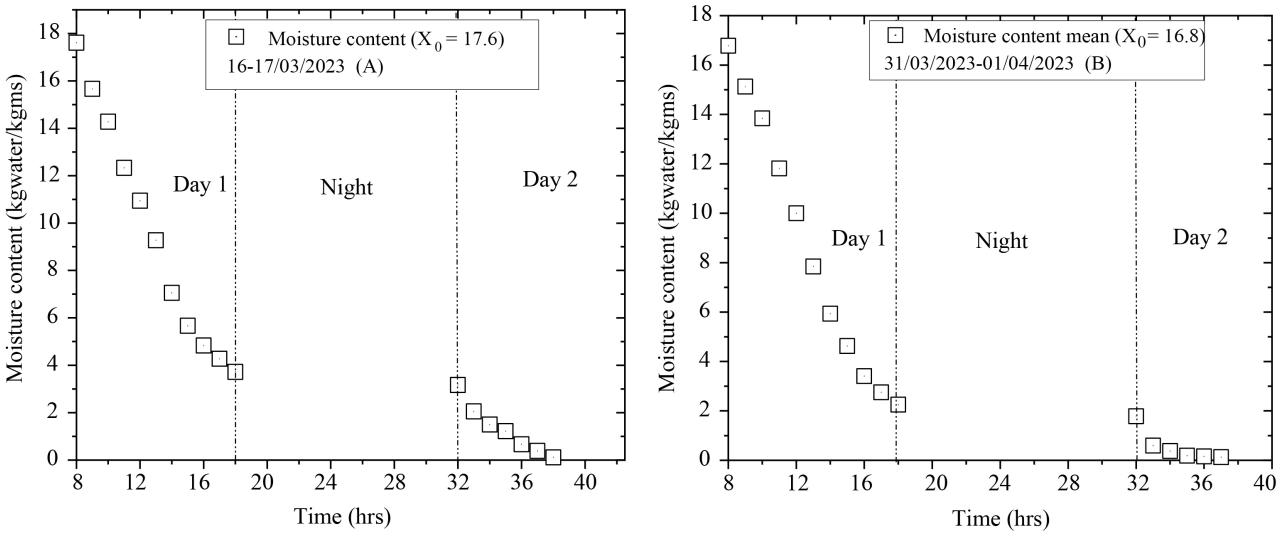

Figure 7. Evolution with time of the average water content of the product during indirect solar drying processes without a thermal storage system.

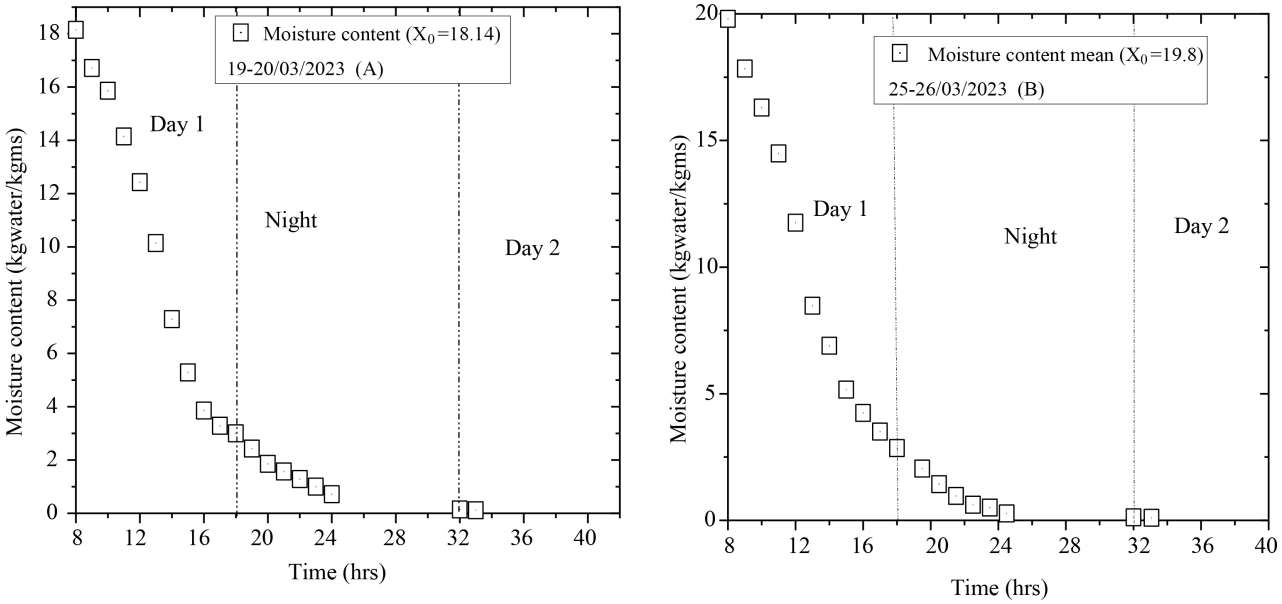

Figure 8. Evolution with time of the average water content of the product during indirect solar drying processes with a thermal storage system.

7.2. Validation of the Drying Kinetics

The calculated values of the statistical parameters used are shown in Table 6 above. The different models are compared on the basis of the values of the coefficient of determination (R^2), the reduced ki-squared (χ^2) and the root mean square error (RMSE). The high value of R^2, and the low values of χ^2 and RMSE reflect a good fit of the model to the experimental values. The values of these parameters range from 0.9287 to 0.9942 for the R^2, from 0.00704 to 0.08641 for the χ^2 and from 0.02797 to 0.09296 for the RMSE. Among these models, the "Page" model gives the highest value of determination R^2 and the lowest ($R^2 = 0.9942$) values of χ^2 and RMSE (respectively and RMSE = 0.00704). It was therefore chosen to represent the behavior of tomato thin-film solar drying kinetics.

Table 6. Statistical parameter values.

Model Name	Model Parameters	R^2	χ^2	RMSE
Lewis	$b = 0.1937$	0.9287	0.08641	0.09296
Henderson and Pabis	$a = 1.107$ $b = 0.2149$	0.9454	0.06615	0.08573
Page	$b = 0.06009$ $n = 1.709$	0.9942	0.00704	0.02797
Logarithmique	$a = 1.703$ $b = 0.09437$ $c = -0.6501$	0.9775	0.02746	0.05859
Two terms	$a = -36.49$ $b = 0.4354$ $c = 37.49$ $d = 0.4229$	0.9456	0.06594	0.09706
Approach of the diffusion	$a = -1.445$ $b = 0.6219$ $c = 0.5268$ $d = 0.6495$	0.9893	0.01298	0.04305
Verma *et al.*	$a = -63.7$ $b = 0.4094$ $c = 0.4032$	0.9879	0.01463	0.04276
Wang and singh	$a = -0.1371$ $b = 0.003889$	0.9757	0.02949	0.05725

Figure 9 and Figure 10 show a comparison of experimental and simulated results for the average dry-base water content of tomatoes from indirect solar drying (Figure 9(a) and Figure 9(b)) and indirect solar drying with thermal energy storage (Figure 10(a) and Figure 10(b)). The evolution of simulated and experi-

mental tomato water contents shows good agreement. Moisture content falls rapidly at the start of the day, stabilizing at the end of the day as drying air temperature and product moisture content decrease. Moisture content falls again when the storage tank is switched on during the night, or on the second day of drying. However, a discrepancy is observed for drying from 03/31/2023 to 04/01/2023. This discrepancy may be due to the fact that the model does not take into account the influence of thermal and hygrometric parameters on the continuation of night drying during indirect solar drying. We can therefore conclude that Page's model provides a satisfactory description of experimental tomato kinetics.

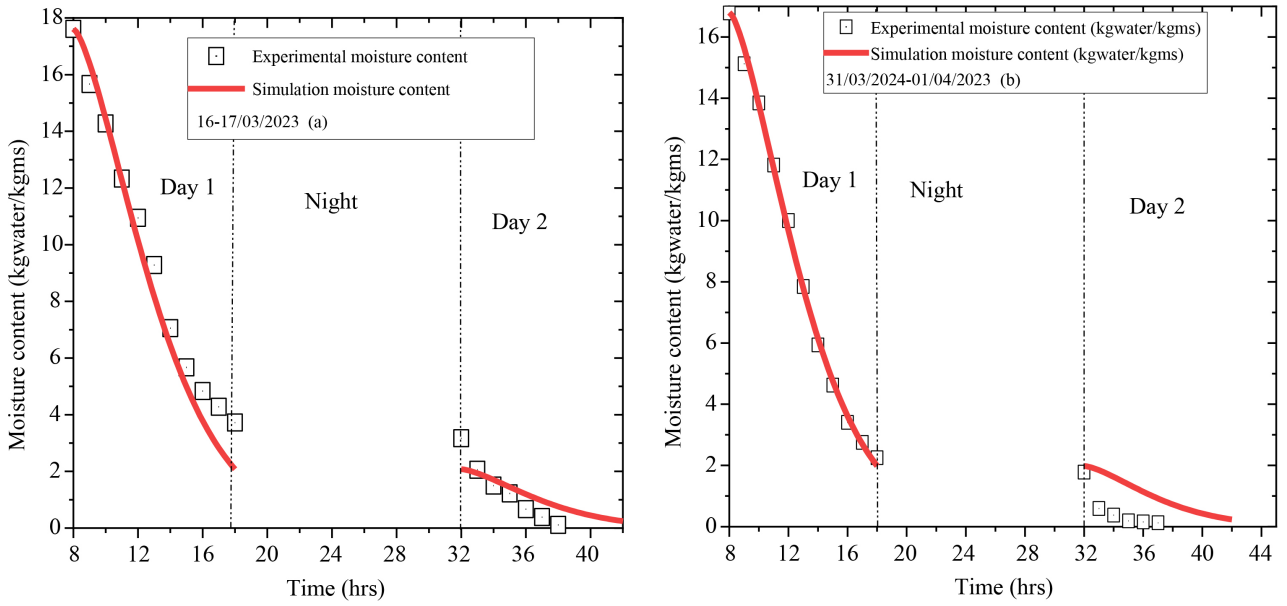

Figure 9. Comparison of simulated and experimental values of tomato water content for 16-17/03/2023 and 31/03/2023-01/04/2023.

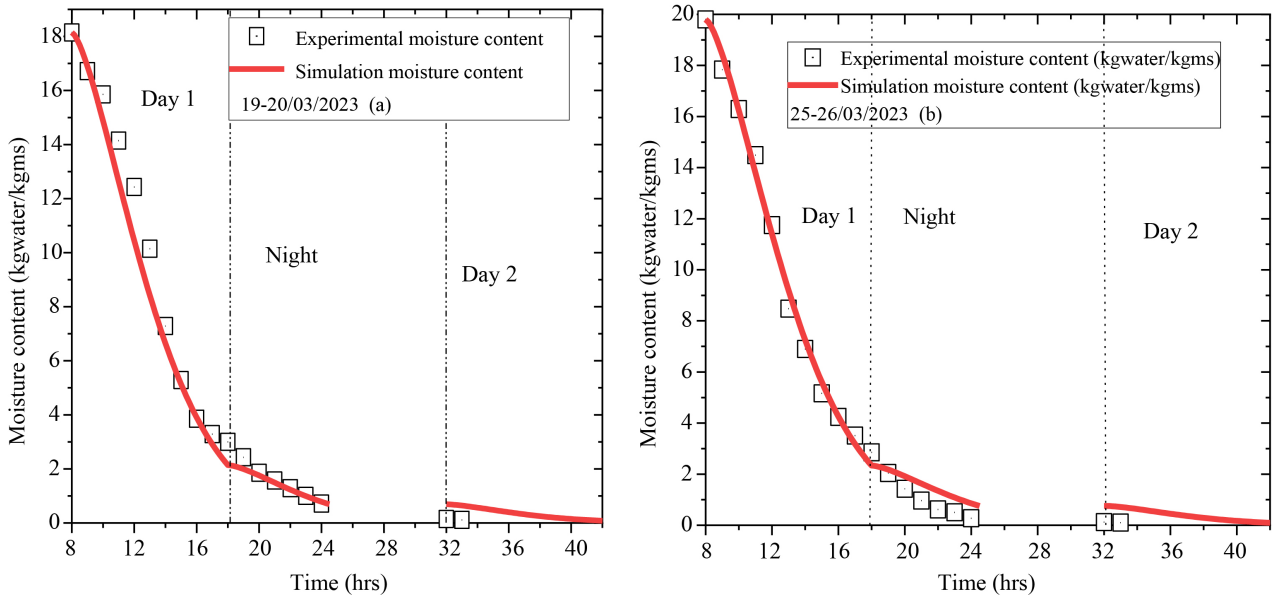

Figure 10. Comparison of simulated and experimental values of tomato water content for 19-20/03/2023 and 25-26/03/202.

8. Conclusion

In this work, indirect solar drying with or without a thin-film tomato storage unit was studied. The drying process was modeled in order to predict the behavior of tomato solar drying kinetics. Eight (08) different thin-film drying models established in the literature were compared on the basis of their correlation coefficients and reduced Ki-squared values. The model validation process was carried out by comparing theoretically calculated water content with experimentally calculated water content. The comparison of theoretical water contents showed good agreement with Page's mathematical model for describing the behavior of tomato solar drying kinetics. Page's model gives a higher value of determination $R^2 = 0.9942$, and lower values of Ki-square $\chi^2 = 0.02797$ and RMSE = 0.00704. This model describes the solar drying behavior of tomatoes under drying air conditions ranging from 26.7˚C to 68.3˚C.

Conflicts of Interest

The authors declare no conflicts of interest regarding the publication of this paper.

References

[1] Toğrul, İ.T. and Pehlivan, D. (2003) Modelling of Drying Kinetics of Single Apricot. *Journal of Food Engineering*, **58**, 23-32. https://doi.org/10.1016/s0260-8774(02)00329-1

[2] Tera, S., Sinon, S., KAM, S., Kayaba, H., Sanogo, O. and Stutz, B. (2024) Study of the Performance of an Indirect Forced Convection Solar Dryer Incorporating a Thermal Energy Storage Device on a Granite Bed for Drying Tomatoes. *Current Journal of Applied Science and Technology*, **43**, 118-127. https://doi.org/10.9734/cjast/2024/v43i74411

[3] El-Sebaii, A.A., Aboul-Enein, S., Ramadan, M.R.I. and El-Gohary, H.G. (2002) Empirical Correlations for Drying Kinetics of Some Fruits and Vegetables. *Energy*, **27**, 845-859. https://doi.org/10.1016/s0360-5442(02)00021-x

[4] Dissa, A.O., Bathiebo, J., Kam, S., Savadogo, P.W., Desmorieux, H. and Koulidiati, J. (2009) Modelling and Experimental Validation of Thin Layer Indirect Solar Drying of Mango Slices. *Renewable Energy*, **34**, 1000-1008. https://doi.org/10.1016/j.renene.2008.08.006

[5] Sacilik, K., Keskin, R. and Elicin, A.K. (2006) Mathematical Modelling of Solar Tunnel Drying of Thin Layer Organic Tomato. *Journal of Food Engineering*, **73**, 231-238. https://doi.org/10.1016/j.jfoodeng.2005.01.025

[6] Badaoui, O., Hanini, S., Djebli, A., Haddad, B. and Benhamou, A. (2019) Experimental and Modelling Study of Tomato Pomace Waste Drying in a New Solar Greenhouse: Evaluation of New Drying Models. *Renewable Energy*, **133**, 144-155. https://doi.org/10.1016/j.renene.2018.10.020

[7] Lamrani, B. and Draoui, A. (2020) Thermal Performance and Economic Analysis of an Indirect Solar Dryer of Wood Integrated with Packed-Bed Thermal Energy Storage System: A Case Study of Solar Thermal Applications. *Drying Technology*, **39**, 1371-1388. https://doi.org/10.1080/07373937.2020.1750025

[8] Elsayed, M.M. (1990) Mathematical Modeling of a Thin Layer Solar Kiln. *Journal of Solar Energy Engineering*, **112**, 196-203. https://doi.org/10.1115/1.2930480

[9] Zahed, A.H. and Elsayed, M.M. (1994) Transient Performance of a Natural Ventilation Solar Kiln. *Renewable Energy*, **4**, 189-198. https://doi.org/10.1016/0960-1481(94)90004-3

[10] Doymaz, İ. (2007) Air-Drying Characteristics of Tomatoes. *Journal of Food Engineering*, **78**, 1291-1297. https://doi.org/10.1016/j.jfoodeng.2005.12.047

[11] Esence, T., Desrues, T., Fourmigué, J., Cwicklinski, G., Bruch, A. and Stutz, B. (2019) Experimental Study and Numerical Modelling of High Temperature Gas/Solid Packed-Bed Heat Storage Systems. *Energy*, **180**, 61-78. https://doi.org/10.1016/j.energy.2019.05.012

[12] Esence, T. (2017) Étude et modélisation des systèmes de stockage thermique de type ré-génératif solide/fluide. Université Grenoble Alpes.

[13] Essalhi, H., Benchrifa, M., Tadili, R. and Bargach, M.N. (2018) Experimental and Theoretical Analysis of Drying Grapes under an Indirect Solar Dryer and in Open Sun. *Innovative Food Science & Emerging Technologies*, **49**, 58-64. https://doi.org/10.1016/j.ifset.2018.08.002

[14] Boughali, S., Benmoussa, H., Bouchekima, B., Mennouche, D., Bouguettaia, H. and Bechki, D. (2009) Crop Drying by Indirect Active Hybrid Solar-Electrical Dryer in the Eastern Algerian Septentrional Sahara. *Solar Energy*, **83**, 2223-2232. https://doi.org/10.1016/j.solener.2009.09.006

[15] Atalay, H. (2019) Performance Analysis of a Solar Dryer Integrated with the Packed Bed Thermal Energy Storage (TES) System. *Energy*, **172**, 1037-1052. https://doi.org/10.1016/j.energy.2019.02.023

Nomenclature

a	external surface area of solids per unit volume of fixed bed, $m^{-2} \cdot m^{-3}$
C_p	heat capacity by mass, $kJ \cdot kg^{-1} \cdot K^{-1}$
D	diameter, m
d_{eq}	diameter solids equivalent, m
e	thickness, m
H	tank height, m
h	convective exchange coefficient, $W \cdot m^{-2} \cdot K^{-1}$
I	solar irradiation, $W \cdot m^{-2}$
k	drying constant
m	mass, kg
$\dot{m}$	fluid mass flow rate, $kg \cdot s^{-1}$
Nu	dimensionless number Nusselt
Re	reynold's dimensionless number
S	tank surface, m^2
T	temperature, K
t	time, s
U	overall heat loss coefficient, $W \cdot m^{-2} \cdot K^{-1}$
u	interstitial fluid velocity, $m \cdot s^{-1}$
v	velocity $m \cdot s^{-1}$
W	thermal front speed, $m \cdot s^{-1}$
X	water content, kg_{water}/kg_{ms}
x	volume fraction of the wall with respect to the fluid
z	axial coordinates in the direction of the fluid, m
Symboles grecs	
λ	thermal conductivity, $W \cdot m^{-1} \cdot K^{-1}$
ρ	density, $kg \cdot m^{-3}$
ε	bedrock porosity
μ	dynamic viscosity, Pa·s
σ	boltzmann constant
ξ	emissivity
Indices et exposants	
a	air
abs	absorber
b	plywood
cap	collector
ciel	sky

cv-ex	convection glass-exterior
cv-abs	convection glass-absorber
cv, abs-f	convection absorber-fluid
cv, iso-ex	convection isolation-extérieur
cv, f-pr	convection fluid-product
cv, f-pint	convection fluid-inner wall
cd, pq-iso	conduction plaque-isolation
cd, pint-pext	conduction inner wall-exterior wall
eq	equivalent
e	tank inlet
eff, f	effective fluid
eff, p	effective wall
eff, s	effective rock
eff, f-s	effective fluid-rock
eff, f-p	effective fluid-wall
ex	external environment
expi	experiment
f	fluid
G	global
i	elementary volume number
iso	isolation
n	drying constant
p	wall
pq	plaque
p,ex	external wall
p,int	inner wall
pr	product
ray, v-ciel	radiation glass-sky
ray, v-abs	radiation glass-absorber
ray, abs-pq	radiation absorber-plaque
ray, abs-pq	radiation absorber-plaque
red, expi	reduction experiment
red, thi	reduction theoretical
red	reduction
s	rock
sech	dryer
t	time
thi	théoretical
v	glass